

1 The *Paulinella* chromatophore transit peptide part2 adopts a 2 structural fold similar to the γ -glutamyl-cyclotransferase fold

3 Victoria Klimenko¹, Jens Reiners², Violetta Applegate², Katharina Reimann¹, Grzegorz
4 Popowicz³, Astrid Hoeppner², Athanasios Papadopoulos², Sander H. J. Smits^{2,4}, Eva C. M.
5 Nowack¹

6 ¹Institute of Microbial Cell Biology, Department of Biology, Heinrich Heine University Düsseldorf,
7 Düsseldorf, Germany

8 ²Center for Structural Studies (CSS), Heinrich Heine University Düsseldorf, Düsseldorf,
9 Germany

10 ³Institute of Structural Biology, Helmholtz Zentrum München, Neuherberg, Germany

11 ⁴Institute of Biochemistry, Heinrich Heine University Düsseldorf, Düsseldorf, Germany

13 **Corresponding author:** Eva C. M. Nowack, email: e.nowack@hhu.de

14 The author responsible for distribution of materials integral to the findings presented in this
15 article in accordance with the policy described in the Instructions for Authors
16 (<https://academic.oup.com/plphys/pages/General-Instructions>) is Eva C. M. Nowack.

18 **Short title:** Structure of the chromatophore transit peptide

20 **Abstract**

21 The chromatophores of the cercozoan amoeba *Paulinella* are photosynthetic organelles that
22 evolved from a cyanobacterial endosymbiont. Many nucleus-encoded chromatophore-targeted
23 proteins carry unusual N-terminal targeting signals termed crTPs, which are bipartite. crTP_{part1}
24 likely mediates trafficking through the secretory pathway and is cleaved off during import, but
25 crTP_{part2} remains attached to its cargo protein and its function is unknown. To unravel the
26 functional role of crTP_{part2}, here we elucidated the structures of crTP_{part2} from two different
27 chromatophore-targeted proteins by X-ray crystallography at \sim 2.3 Å resolution. Interestingly, the
28 crTP_{part2} of both proteins adopts a structural fold. Both structures share a conserved structured
29 core and a flexible N-terminal arm. The structured core resembles proteins of the γ -glutamyl
30 cyclotransferase superfamily within which crTP_{part2} structures form a protein (sub)-family. The
31 proposed catalytic center typical for proteins with cyclotransferase activity is not conserved in
32 crTP_{part2}. A Cys pair that is conserved in crTP_{part2} of many chromatophore-targeted proteins has
33 been captured as a disulfide bridge. Together, our data suggest that chromatophore-targeted

© The Author(s) 2025. Published by Oxford University Press on behalf of American Society of Plant Biologists. This
is an Open Access article distributed under the terms of the Creative Commons Attribution-NonCommercial-
NoDerivs licence (<https://creativecommons.org/licenses/by-nc-nd/4.0/>), which permits non-commercial
reproduction and distribution of the work, in any medium, provided the original work is not altered or transformed
in any way, and that the work is properly cited. For commercial re-use, please contact reprints@oup.com for
reprints and translation rights for reprints. All other permissions can be obtained through our RightsLink service via
the Permissions link on the article page on our site—for further information please contact
journals.permissions@oup.com.

1 proteins are imported in their folded state and that the fold adopted by crTP_{part2} plays a
2 functional role during import. The characterization of its structure and flexibility provides
3 important steps towards elucidating this protein translocation mechanism.

4

5 **Introduction**

6 The transformation of bacterial endosymbionts into eukaryotic organelles has been a key
7 process in eukaryote evolution. The only organelles identified so far that evolved by primary
8 endosymbiosis events that were independent of the events that gave rise to mitochondria and
9 plastids, are the photosynthetic “chromatophores” of the cercozoan amoeba *Paulinella* and the
10 nitrogen-fixing “nitroplasts” of the haptophyte *Braarudosphaera*. In both cases, following the
11 establishment of a cyanobacterial endosymbiont, the endosymbiont lost many functions by
12 reductive genome evolution that were compensated by the import of nucleus-encoded proteins
13 (Nowack and Grossman, 2012; Singer et al., 2017; Coale et al., 2024). Many of these organelle-
14 targeted proteins carry conserved sequence extensions that apparently function as unique types
15 of targeting signals (Singer et al., 2017; Coale et al., 2024). Their way of functioning is little
16 understood.

17 In *Paulinella chromatophora*, the subject of this study, long chromatophore-targeted proteins
18 [ICTPs; typically >250 amino acids (aa)] carry such N-terminal targeting signals that are referred
19 to as ‘chromatophore transit peptides’ (crTPs) (Singer et al., 2017). CrTPs are ~200 aa long,
20 contain conserved sequence elements, and are bipartite. Upon import, crTP_{part1} is cleaved off,
21 whereas crTP_{part2} remains attached to the N-terminus of most ICTPs (Oberleitner et al., 2022)
22 (**Fig. 1A**). It has been proposed that the conserved hydrophobic helix in crTP_{part1} anchors crTP-
23 carrying proteins co-translationally in the ER membrane in an N-terminus out, C-terminus in
24 conformation and that the N-terminal adaptor protein 1 complex binding site (AP-1 BS) is
25 responsible for packaging ICTPs into clathrin-coated vesicles (Oberleitner et al., 2022).
26 Although the exact timepoint at which crTP_{part1} is cleaved off is unknown, it is reasonable to
27 assume that cleavage happens after this sorting step, possibly following fusion of the vesicles
28 with the outer (host-derived) chromatophore membrane (Sørensen et al., 2025). This would
29 result in a release of the cargo proteins, still attached to crTP_{part2}, into the intermembrane space.
30 The function of crTP_{part2} is unclear, but it is likely involved in mediating protein translocation
31 across the two remaining layers (i.e., peptidoglycan (PG) and inner membrane).

32 Interestingly, crTP_{part2} contains conserved predicted secondary structure elements across
33 proteins (Oberleitner et al., 2022), suggesting that, different from the N-terminal transit peptides
34 of mitochondrion and plastid-targeted proteins, which are generally unstructured, crTP_{part2}
35 adopts a structural fold. This hypothesis guided the experimentation in this study.

36

37

38

39

1 **Results**2 **CrTP_{part2} adopts a structured fold**

3 To contribute to the understanding of the function of crTP_{part2}, we aimed to elucidate its 3D
 4 structure. For this purpose, we focused on crTP_{part2} from three chromatophore-targeted proteins.
 5 These were derived from the transcripts scaffold2581, scaffold7023, and scaffold4337
 6 (GenBank accessions: GEZN01002575.1, GEZN01007010.1, and GEZN01004327.1, (Nowack
 7 et al., 2016)) encoding a predicted RNA helicase (RnaH), N-acetyl-gamma-glutamyl-phosphate
 8 reductase (ArgC), and cysteine synthase A (CysK); from here on crTP_{part2_RnaH}, crTP_{part2_ArgC}, and
 9 crTP_{part2_CysK}, respectively (**Fig. 1A**). Initial analyses of these proteins by AlphaFold3 (Abramson
 10 et al., 2024) predicted the structures of the cargo proteins, RnaH, ArgC, and CysK, with high
 11 confidence; however, the crTP structures could not be modeled in high quality and resulted in
 12 largely unstructured domains (**Fig. S1**). Hence, we aimed for structure characterization by X-ray
 13 crystallography. To this end, we purified recombinant crTP_{part2_RnaH}, crTP_{part2_ArgC}, and
 14 crTP_{part2_CysK}-containing constructs following their overexpression in *Escherichia coli* (**Fig. S2-S3**). Two of these proteins, crTP_{part2_RnaH} and crTP_{part2_ArgC}, readily formed crystals of sufficient
 15 quality to determine their structure via X-ray crystallography, at 2.4 Å and 2.2 Å resolution,
 16 respectively (for details see **Suppl. Text** and **Table S1**). The quality of the electron density map
 17 is visualized in **Fig. S4**.

19 Both structures contain a structured core (colored gold in **Fig. 1B, C**) and a mostly
 20 unstructured N-terminal arm (blue in **Fig. 1B, C**). The structured cores consist of a five-stranded
 21 antiparallel β-barrel (β1-β3-β2-β4-β5) flanked by an α-helix (α2), decorated by connecting loops.
 22 In crTP_{part2_RnaH}, additional very short β-strands (β1', β2') and α-helical elements (α1'- α3') are
 23 embedded into the connecting loops. The N-terminal arm clearly adopts a different conformation
 24 in both structures, indicating that this part might be flexible, whereas the structured core is
 25 almost identical between crTP_{part2_RnaH} and crTP_{part2_ArgC} over a large part of the structure (rmsd
 26 0.7 Å over 63 aligned Cα atoms, **Fig. 1D**). In crTP_{part2_RnaH}, the β-barrel is stabilized by a
 27 disulfide bridge formed between Cys113 and Cys169 (**Fig. 1E**). This Cys pair is conserved in
 28 many, but not in all crTP sequences, however, if Cys occurs in these positions, it occurs as a
 29 pair (see asterisks in **Fig. 1A**). The loop connecting helix α2 with β4 is much larger in
 30 crTP_{part2_RnaH} when compared to crTP_{part2_ArgC}. The loops connecting β2 and β3 as well as α2 with
 31 β3 are similar in length but adopt different conformations in the two structures, hinting towards
 32 flexibility at these positions whereas the core is rigid.

33 In crTP_{part2_ArgC}, the N-terminal arm interacts via hydrophobic interactions between Phe64
 34 and Trp110 as well as Ile70 and Tyr112 with the structured core and hence, shows a “closed
 35 conformation” (**Fig. 1F**). These hydrophobic residues are highly conserved between different
 36 crTP sequences (black arrowheads in **Fig. 1A**). In crTP_{part2_RnaH}, for which the “open
 37 conformation” of the N-terminal arm was captured, the hydrophobic residues are exposed (**Fig.**
 38 **1E**). This open conformation appears to be stabilized by the formation of a crystallographic
 39 dimer (**Fig. S5**). The N-terminal arm contains several proline residues, which give the arm a
 40 specific conformation. To verify the flexibility of the N-terminal arm, we applied molecular
 41 simulations using the program CABS Flex with the all-atom reconstruction implemented

1 (Wróblewski et al., 2025). Here, crTP_{part2_RnaH} shows high flexibility at the N-terminus in
 2 comparison with the N-terminus of crTP_{part2_ArgC} (**Fig. S6**). Interestingly, in both structures,
 3 flexibility peaks in the proline-rich region, which might function as a hinge for flexibility. Together
 4 these results suggest that the N-terminal arm can adopt several conformations, however, in the
 5 closed conformation is stabilized by the interactions described above.

6 Notably, N-terminal crTPs are also found in ICTPs of *Paulinella micropora*, a
 7 chromatophore-containing sister of *P. chromatophora* (Lhee et al., 2021). To assess whether
 8 the structural features identified in crTPs of *P. chromatophora* are conserved across species,
 9 we aligned the sequences of the three crTPs studied here with those of crTPs from *P.*
 10 *micropora* (**Fig. S7A**). Intriguingly, all important structural features identified in *P.*
 11 *chromatophora* are conserved in *P. micropora* including, in crTP_{part1}, the AP-1 BS and
 12 hydrophobic helix; and, in crTP_{part2}, the Cys-pair, the hydrophobic residues supporting
 13 interactions between flexible arm and structured core, and the proline-rich region (**Fig. S7A**).
 14 Furthermore, homology models obtained using the solved crystal structures of crTP_{part2_RnaH} and
 15 crTP_{part2_ArgC} as templates, suggest that crTP_{part2} in *P. micropora* can adopt similar folds (**Fig.**
 16 **S7B-C**). However, the predictive value of these models is low, since -as observed before for
 17 AlphaFold3 (**Fig. S1**)- the quality estimates for all homology models obtained were very low
 18 (see **Fig. S7B-C** and corresponding figure legend). To study crTP_{part2} linked to their natural
 19 cargo proteins, we purified recombinant crTP_{part2_RnaH}-RnaH and crTP_{part2_ArgC}-ArgC following
 20 their production in *E. coli* (**Fig. S2-S3**). However, despite several attempts, these proteins did
 21 not form crystals.

22

23 **SAXS measurements indicate flexibility of the N-terminal arm and the linker to the cargo 24 protein in solution**

25 To investigate the flexibility of crTP_{part2} in solution as well as the spatial arrangement between
 26 the crTP_{part2} regions and their cargo proteins, we performed small angle X-ray scattering (SAXS)
 27 measurements. These measurements demonstrated that crTP_{part2_ArgC}, crTP_{part2_RnaH}, and
 28 crTP_{part2_CysK} alone are monomeric in solution (**Tables S2-S3** and **Suppl. Text**). For
 29 crTP_{part2_RnaH}, the “open conformation” of the flexible arm, found in the crystal dimer packing, is
 30 also present in solution. Here the flexible arm adopts, as expected, multiple conformations (see
 31 **Suppl. Text**). Flexibility analyses of the termini with the Ensemble Optimization Method (EOM)
 32 revealed four different conformations that all represent different “open conformations”, but no
 33 indication for a “closed conformation” for crTP_{part2_RnaH} (**Fig. 2A, B** and **Fig. S8**). In comparison,
 34 neither crTP_{part2_ArgC}, nor crTP_{part2_CysK} showed flexible termini and show a more compact
 35 conformation (**Figs. S9-S10** and **Suppl. Text**).

36 CrTP_{part2_RnaH}-RnaH, too, is a monomer in solution (**Table S2**) and we recovered three
 37 distinct conformations, indicating flexibility between the crTP_{part2_RnaH} domain and the attached
 38 cargo protein, RnaH (**Fig. 2C**, **Fig. S11** and **Suppl. Text**). In contrast, crTP_{part2_ArgC}-ArgC
 39 appears dimeric over the whole concentration range (**Table S2**) with the dimer interface
 40 predicted within the cargo protein ArgC. The models obtained showed that crTP_{part2_ArgC}-ArgC
 41 forms an overall compact molecule, but, again, reveals flexibility between the crTP_{part2} domain

1 and the attached cargo protein (**Fig. 2D** and **Fig. S12**). Furthermore, the N-terminal arm of
 2 $\text{crTP}_{\text{part2_ArgC}}$ which appeared “closed” in the monomer crystal and in-solution model of
 3 $\text{crTP}_{\text{part2_ArgC}}$ alone, now remains flexible, more in line with an “open conformation” (for more
 4 details see **Suppl. Text**).

5

6 **The structured core of $\text{crTP}_{\text{part2}}$ shows similarity to γ -glutamyl cyclotransferase fold**
 7 **proteins**

8 Searching the coordinates of the solved $\text{crTP}_{\text{part2}}$ structures against the PDB database using the
 9 DALI server (<http://ekhidna2.biocenter.helsinki.fi/dali/>) revealed similarity of both structures to
 10 members of the γ -glutamyl cyclotransferase-like superfamily (InterPro entry IPR036568) (**Table**
 11 **S4**). This superfamily contains five protein families, the γ -glutamyl cyclotransferase (GGCT), the
 12 γ -glutamylamine cyclotransferase (GGACT), the glutathione-specific GGCT (GCG or ChaC), the
 13 BrtG-like, and the plant-specific GGCT-like family [**Fig. 3** and (Kumar et al., 2015)].

14 For 10 members of the GGCT-like superfamily structures have been experimentally
 15 solved (**Fig. 3A** and **Table S5**). Highest similarity scores were obtained for the *S. cerevisiae*
 16 glutathione-specific GGCT ChaC (pdb id: 5hwi, z-scores = 10.3 and 9.3, sequence identities =
 17 13 and 17%), the human GGCT (pdb id: 2i5t, z-scores = 9.1 and 8.6, sequence identities = 15
 18 and 23%), and the *B. subtilis* protein YkqA (pdb id: 2qik, z-scores = 9.2 and 8.0, sequence
 19 identities 18 and 23%) (values for $\text{crTP}_{\text{part2_RnAH}}$ and $\text{crTP}_{\text{part2_ArgC}}$, respectively). Thus, structure
 20 comparison did not reveal affiliation of the $\text{crTP}_{\text{part2}}$ structures to any particular family within the
 21 superfamily. In line with this result, a maximum likelihood (ML) phylogenetic analysis of a
 22 structure-guided alignment resolves $\text{crTP}_{\text{part2}}$ sequences as a unique family within IPR036568
 23 that forms a short common branch with the plant-specific GGCT-like family (**Fig. 3A**).

24 For several proteins of the superfamily, enzymatic activities have been characterized
 25 and a common function of many is the cleavage of diverse γ -glutamyl derivatives by
 26 cyclotransferase activity (**Suppl. Text**). Despite their low sequence identities, catalysis is based
 27 on a similar structural fold, which includes a cavity between the β -barrel and adjacent helix that
 28 contains a conserved YGSL motif and a Glu residue that likely represents the active site
 29 (Oakley et al., 2010; Chi et al., 2014). The $\text{crTP}_{\text{part2}}$ structures form a similar cavity build by
 30 strand β 1 and β 5, helix α 2, and the loop between β 1 and β 2 that aligns with the proposed
 31 substrate-binding cavity in the human GGACT (3jub, 3juc) (Oakley et al., 2010) (**Fig. 3B**). The
 32 YGSL motif is partly conserved in $\text{crTP}_{\text{part2}}$. Tyr99 of $\text{crTP}_{\text{part2_ArgC}}$ at the N-terminal end of the
 33 loop connecting β 1 and β 2 corresponds to Tyr7 in the YGSL motif of the human GGACT. This
 34 Tyr residue is conserved throughout different $\text{crTP}_{\text{part2}}$ sequences (**Fig. S13**) and its side chain
 35 is orientated towards the inside of the cavity (**Fig. 3C**). The following Gly is found only in around
 36 half of the $\text{crTP}_{\text{part2}}$ sequences and is replaced in the remaining sequences mostly by other
 37 small amino acids (A, S, T, P). Ser and Leu of the YGSL motif are conserved in $\text{crTP}_{\text{part2_RnAH}}$ but
 38 non-conservatively replaced in $\text{crTP}_{\text{part2_ArgC}}$ by Glu and Asp. Finally, Glu82 of the human
 39 GGACT that sits at the C-terminal end of cavity-delimiting helix with its side chain oriented
 40 towards the inside of the cavity has been proposed to form the catalytic center (Oakley et al.,

1 2010). Glu in this position is highly conserved in many proteins of the superfamily (**Fig. S13**).
2 Interestingly, in crTP_{part2}_ArgC and crTP_{part2}_RnaH this catalytic Glu is replaced by a Tyr and an Arg,
3 respectively (**Fig. 3D** and **Fig. S13**). In other crTP_{part2} sequences, this site harbors several other
4 aa residues (see alignment position 192 in **Fig. 1A**). Hence, it appears unlikely that crTP_{part2} has
5 cyclotransferase activity.

6

7 Discussion

8 Here we showed that crTP_{part2} domains of ICTPs in *P. chromatophora* adopt a structured fold
9 that consists of a structured core with similarity to GGCT-like proteins and an N-terminal flexible
10 arm that can interact via conserved hydrophobic residues with the structured core (see arrow
11 heads in **Fig. 1A**). The proline-rich region in the N-terminal arm may represent an anchor for an
12 interaction partner, since proline-rich regions within other proteins are known to form interaction
13 surfaces that are responsible for interactions with e.g. elements of the cytoskeleton,
14 peptidoglycan or biological membranes (Williamson, 1994). Interaction with a potential partner
15 would be facilitated by the inferred flexibility of the N-terminal arm as well as the linker between
16 crTP_{part2} and its cargo protein (**Fig. 2**). The disulfide bridge in crTP_{part2}_RnaH that has been
17 captured by crystallography (**Fig. 1E**) is formed by a Cys pair that is conserved across crTP_{part2}
18 domains of diverse ICTPs, which suggests that the oxidized state is biologically relevant. This
19 assumption is in line with the oxidizing conditions in the ER lumen (Margittai et al., 2015) that
20 has been suggested as intermediate station in the ICTP import pathway (Oberleitner et al.,
21 2022).

22 Interestingly, whereas ICTPs apparently require a crTP for import, short chromatophore-
23 targeted proteins (sCTPs; typically <90 aa) that also apparently traffic into the chromatophore
24 via the Golgi (Nowack and Grossman, 2012) lack similar targeting signals (Singer et al., 2017).
25 Since ICTPs and sCTPs comprise overlapping functions [e.g., cytosolic metabolic enzymes,
26 diverse DNA-binding proteins (Singer et al., 2017; Oberleitner et al., 2020; Macorano et al.,
27 2023)], requirement of a crTP does not seem to be tied to a specific function or final localization
28 of the cargo protein but rather its size. This size cutoff could be set by the - so far unknown -
29 import gate in the inner chromatophore membrane or the mesh size of the PG sacculus.

30 In *E. coli*, a size cutoff of ~50 kDa has been estimated for globular proteins to be able to
31 diffuse through the stretched PG sacculus (Demchick and Koch, 1996). Cyanobacteria generally
32 feature a thicker PG with a much higher degree of crosslinking (Hoiczyk and Hansel, 2000).
33 Hence, although PG composition and crosslinking has not been analyzed for chromatophores
34 yet, it might represent an important hurdle for the transport of folded ICTPs which reach sizes
35 >100 kDa (Singer et al., 2017). Also the plastids of Glaucophytes retained a pronounced PG
36 layer; however, they use a TIC/TOC translocon-based mechanism for importing plastid-targeted
37 pre-proteins in an unfolded state and only the mature stromal proteins fold into their functional
38 conformation (Steiner and Löffelhardt, 2002). Hence, the PG does not represent a relevant size
39 cutoff here.

1 Since many GGCT-family proteins cleave γ -glutamyl-containing peptides, the γ -glutamyl-
2 containing muropeptides that cross link the PG appeared as possible ligands of crTP_{part2}.
3 Although cleavage of these peptides by crTP_{part2} appears unlikely due to the lack of
4 conservation of the proposed catalytic center (Fig. 3D), we hypothesized that the binding to
5 muropeptide derivatives could be involved in recognition of non-crosslinked areas in the PG
6 and/or result in a conformational change enabling interaction with interaction partners at the
7 inner membrane. However, we could not experimentally confirm binding of crTP_{part2} to the *E. coli*
8 PG penta or tetrapeptide. Hence, if muropeptides are the natural ligands of crTP_{part2}, we could
9 not identify the exact ligand and/or correct conditions yet under which binding occurs.

10 In sum, our data suggests that ICTPs are imported in their folded state and that the fold
11 adopted by crTP_{part2} plays an as of yet unknown functional role in the import process that
12 appears to be conserved cross chromatophore-containing *Paulinella* species. The
13 characterization of its structure and flexibility provides important steps towards unraveling this
14 protein translocation mechanism.

15

16 Materials and Methods

17 **Cultivation of *P. chromatophora* and synthesis of complementary DNA (cDNA).** *P.*
18 *chromatophora* CCAC0185 was grown as described before (Nowack et al., 2016). Total RNA
19 was extracted and cDNA prepared as described in (Macorano et al., 2023).

20 **Construction of expression plasmids.** The crTP_{part2} domains alone or crTP_{part2} domains plus
21 their cargo proteins were cloned into the expression vector GPN131. This vector is a derivative
22 of the plasmid pET-22b(+) (Novagene; 69744), in which the pelB sequence and C-terminal His₆-
23 tag were replaced by an N-terminal His₆-tag, thrombin cleavage site, and SUMO-tag. For details
24 see the **Suppl. Text, Fig. S14, and Table S6**.

25 **Heterologous expression of recombinant proteins.** For overexpression of the constructs
26 His₆-SUMO-TEV-crTP_{part2_RnaH}, His₆-SUMO-TEV-crTP_{part2_ArgC}, His₆-SUMO-TEV-crTP_{part2_CysK},
27 His₆-SUMO-TEV-crTP_{part2_ArgC-ArgC}, and His₆-SUMO-TEV-crTP_{part2_RnaH-RnaH} (see Fig. S2A),
28 plasmids GPN142, GPN167, GPN168, GPN195, and GPN194, respectively, were individually
29 transformed into *E. coli* strain LOBSTR-BL21(DE3)-RIL (Kerafast, Boston, MA) (Andersen et al.,
30 2013) and proteins were expressed under conditions detailed in the **Suppl. Text**. Finally, cells
31 were harvested, pellets flash frozen and stored at -80°C until use.

32 **Protein purification.** Frozen cells from expression cultures were lysed and the His₆-SUMO-
33 tagged proteins of interest isolated by immobilized metal ion chromatography (IMAC). The His₆-
34 SUMO tag was cleaved of by TEV protease and the proteins of interest purified by reverse
35 IMAC followed by size exclusion chromatography (SEC). For details see the **Suppl. Text**.
36 Protein amounts were determined by a nanophotometer (NP80, Implen). Obtained fractions
37 were analyzed by SDS-PAGE under denaturing conditions on 12.5% polyacrylamide
38 (ROTIPHORESE® 30; 29:1; Roth) Tris-glycine gels (Schägger, 2006) (Fig. S2) and BN PAGE

1 on 4-16% gels (SERVA, SERVAGel™ N 4 - 16 Cat. No. 43204) according to the manufacturer's
2 recommendations (Fig. S3), both stained with Coomassie Brilliant Blue R250.

3 **Protein crystallization and 3D structure determination by X-ray crystallography.**
4 CrTP_{part2_RnaH} was crystallized at 12°C with 1.5 µl of 12 mg/ml protein in buffer A (see **Suppl.**
5 **Text**), mixed with 1.5 µl 23% PEG 3350 in 0.1 M HEPES pH 8.5. CrTP_{part2_ArgC} was crystallized
6 at 12°C with 0.1 µl of 12 mg/ml protein in buffer A mixed with 0.1 µl 0.1 M HEPES pH 6.5, 2.4 M
7 AmSO₄ (final pH 7). Diffraction data from obtained crystals of both proteins were collected at the
8 P13 beamline (PETRA III, DESY Hamburg) (Cianci et al., 2017). More details on
9 experimentation, data collection, and refinement statistics are reported in **Table S1** and the
10 **Suppl. Text**. Figures were generated using PyMOL (Schrodinger LLC; www.pymol.org).

11 **Small-angle X-ray scattering.** SAXS data of crTP_{part2_RnaH}, crTP_{part2_ArgC}, and crTP_{part2_CysK} were
12 collected on the P12 beamline at PETRA III, DESY, Hamburg) (Blanchet et al., 2015), and of
13 crTP_{part2_ArgC}-ArgC and crTP_{part2_RnaH}-RnaH on our Xeuss 2.0 Q-Xoom system from Xenocs.
14 Primary data reduction was performed with the program PRIMUS (Konarev et al., 2003). With
15 the Guinier approximation (Guinier, 1939) implemented in PRIMUS, we determine the forward
16 scattering $I(0)$ and the radius of gyration (R_g) and used the program GNOM (Svergun, 1992) to
17 estimate the maximum particle dimension (D_{max}) with the pair-distribution function $p(r)$.
18 Comparison of the theoretical scattering intensity of the solved crystal structures against the
19 experimental scattering data was done with CRYSTAL (Svergun et al., 1995). Flexible parts of
20 the proteins were analyzed using EOM (Bernadó et al., 2007; Tria et al., 2015) and rigid body
21 modeling with CORAL (Petoukhov et al., 2012). Details are provided in the **Suppl. Text** and
22 **Table S2**.

23 **Phylogenetic analysis.** Sequences of crTP_{part2} from indicated transcripts were aligned with
24 diverse GGCT-like superfamily proteins downloaded from NCBI. A structure-guided alignment
25 was generated using PROMALS3D (Pei et al., 2008). The ML tree was inferred with iqtree2
26 (Nguyen et al., 2015; Minh et al., 2020) using automatic model selection and 1000 ultrafast
27 bootstrap replicates.

28

29 **Accession Numbers**

30 Sequence data from this article can be found in the GenBank/EMBL data libraries under
31 accession numbers _GEZN01002575.1, GEZN01007010.1, and GEZN01004327.1.

32 **Data availability**

33 Solved protein structures were deposited in the Worldwide Protein Data Bank
34 (https://www.rcsb.org) with accession codes provided in **Table S1**. SAXS data were uploaded to
35 the Small Angle Scattering Biological Data Bank (SASBDB) (Kikhney et al., 2020) with
36 accession codes provided in **Table S2**.

37

1 **Acknowledgements**

2 We acknowledge DESY (Hamburg, Germany), a member of the Helmholtz Association HGF, for
3 provision of experimental facilities. Parts of this research were carried out at PETRA III and we
4 thank Tobias Gräwert, Dmytro Soloviov, and Cy M. Jeffries (EMBL Hamburg) for assistance in
5 using beamline P12 and Gleb Bourenkov for P13. We thank the beamline scientist from ID23-
6 eh1 at the ESRF Grenoble for their help in the initial stages of this project where the initial
7 crystals were tested, and Christian Mammen and Alice Pawlowski for their help with the BN
8 PAGE.

9

10 **Author contributions**

11 V.K., J.R., S.H.J.S., and E.C.M.N. designed the research; all authors performed research and
12 analyzed data; V.A. and A.H. crystalized the proteins; A.P. performed SEC-MALS experiments;
13 E.C.M.N., S.H.J.S, and J.R. wrote the paper with contributions of all co-authors.

14

15 **Funding**

16 This work was partially funded by SFB 1208 of the DFG, Project ID 267205415 (to ECMN),
17 SFB1535 of the DFG, Project ID 458090666 (to SHJS). The Center for Structural Studies is
18 funded by the DFG (Grant number 417919780 and INST 208/761-1 FUGG, INST 208/740-1
19 FUGG, and INST 208/868-1 FUGG to SS).

20

21 **References**

22 Abramson J, Adler J, Dunger J, Evans R, Green T, Pritzel A, Ronneberger O, Willmore L, Ballard AJ,
23 Bambrick J, Bodenstein SW, Evans DA, Hung CC, O'Neill M, Reiman D, Tunyasuvunakool K, Wu
24 Z, Zemgulyte A, Arvaniti E, Beattie C, Bertolli O, Bridgland A, Cherepanov A, Congreve M,
25 Cowen-Rivers AI, Cowie A, Figurnov M, Fuchs FB, Gladman H, Jain R, Khan YA, Low CMR, Berlin
26 K, Potapenko A, Savy P, Singh S, Stecula A, Thillaisundaram A, Tong C, Yakneen S, Zhong ED,
27 Zielinski M, Zídek A, Bapst V, Kohli P, Jaderberg M, Hassabis D, Jumper JM (2024) Accurate
28 structure prediction of biomolecular interactions with AlphaFold 3. *Nature* **630**: 493-500

29 Andersen KR, Leksa NC, Schwartz TU (2013) Optimized *E. coli* expression strain LOBSTR eliminates
30 common contaminants from His-tag purification. *Proteins: Structure, Function and*
31 *Bioinformatics* **81**: 1857-1861

32 Bernadó P, Mylonas E, Petoukhov MV, Blackledge M, Svergun DI (2007) Structural characterization of
33 flexible proteins using small-angle X-ray scattering. *Journal of the American Chemical Society*
34 **129**: 5656-5664

35 Blanchet CE, Spilotros A, Schwemmer F, Graewert MA, Kikhney A, Jeffries CM, Franke D, Mark D,
36 Zengerle R, Cipriani F, Fiedler S, Roessle M, Svergun DI (2015) Versatile sample environments
37 and automation for biological solution X-ray scattering experiments at the P12 beamline (PETRA
III, DESY). *Journal of Applied Crystallography* **48**: 431-443

1 **Chi ZK, Byrne ST, Dolinko A, Harraz MM, Kim MS, Umanah G, Zhong J, Chen R, Zhang JM, Xu JC, Chen L,**
2 **Pandey A, Dawson TM, Dawson VL** (2014) Botch is a gamma-glutamyl cyclotransferase that
3 deglycinates and antagonizes Notch. *Cell Reports* **7**: 681-688

4 **Cianci M, Bourenkov G, Pompidor G, Karpics I, Kallio J, Bento I, Roessle M, Cipriani F, Fiedler S,**
5 **Schneider TR** (2017) P13, the EMBL macromolecular crystallography beamline at the low-
6 emittance PETRA III ring for high- and low-energy phasing with variable beam focusing. *Journal of Synchrotron Radiation* **24**: 323-332

7 **Coale TH, Loconte V, Turk-Kubo KA, Vanslembrouck B, Mak WKE, Cheung S, Ekman A, Chen J-H,**
8 **Hagino K, Takano Y, Nishimura T, Adachi M, Le Gros M, Larabell C, Zehr JP** (2024) Nitrogen-
9 fixing organelle in a marine alga. *Science* **384**: 217-222

10 **Demchick P, Koch AL** (1996) The permeability of the wall fabric of *Escherichia coli* and *Bacillus subtilis*.
11 *Journal of Bacteriology* **178**: 768-773

12 **Guinier A** (1939) Small-angle X-ray diffraction: application to the study of ultramicroscopic phenomena.
13 *Annales de Physique* **11**: 161-237

14 **Hoiczyk E, Hansel A** (2000) Cyanobacterial cell walls: News from an unusual prokaryotic envelope.
15 *Journal of Bacteriology* **182**: 1191-1199

16 **Kikhney AG, Borges CR, Molodenskiy DS, Jeffries CM, Svergun DI** (2020) SASBDB: Towards an
17 automatically curated and validated repository for biological scattering data. *Protein Sci* **29**: 66-
18 75

19 **Konarev PV, Volkov VV, Sokolova AV, Koch MHJ, Svergun DI** (2003) PRIMUS: a Windows PC-based
20 system for small-angle scattering data analysis. *Journal of Applied Crystallography* **36**: 1277-
21 1282

22 **Kumar S, Kaur A, Chattopadhyay B, Bachhawat AK** (2015) Defining the cytosolic pathway of glutathione
23 degradation in *Arabidopsis thaliana*: role of the ChaC/GCG family of gamma-glutamyl
24 cyclotransferases as glutathione-degrading enzymes and AtLAP1 as the Cys-Gly peptidase.
25 *Biochemical Journal* **468**: 73-85

26 **Lhee D, Lee J, Ettahi K, Cho CH, Ha JS, Chan YF, Zelzion U, Stephens TG, Price DC, Gabr A, Nowack ECM,**
27 **Bhattacharya D, Yoon HS** (2021) Amoeba genome reveals dominant host contribution to plastid
28 endosymbiosis. *Molecular Biology and Evolution* **38**: 344-357

29 **Macorano L, Binny TM, Spiegl T, Klimenko V, Singer A, Oberleitner L, Applegate V, Seyffert S, Stefanski**
30 **A, Gremer L, Gertzen CGW, Höppner A, Smits SHJ, Nowack ECM** (2023) DNA-binding and
31 protein structure of nuclear factors likely acting in genetic information processing in the
32 *Paulinella* chromatophore. *Proc. Natl. Acad. Sci. USA* **120**: e2221595120

33 **Margittai É, Enyedi B, Csala M, Geiszt M, Bánhegyi G** (2015) Composition of the redox environment of
34 the endoplasmic reticulum and sources of hydrogen peroxide. *Free Radical Biology and*
35 *Medicine* **83**: 331-340

36 **Minh BQ, Schmidt HA, Chernomor O, Schrempf D, Woodhams MD, von Haeseler A, Lanfear R** (2020)
37 IQ-TREE 2: New models and efficient methods for phylogenetic inference in the genomic era.
38 *Molecular Biology and Evolution* **37**: 1530-1534

39 **Nguyen LT, Schmidt HA, Von Haeseler A, Minh BQ** (2015) IQ-TREE: A fast and effective stochastic
40 algorithm for estimating maximum-likelihood phylogenies. *Molecular Biology and Evolution* **32**:
41 268-274

42 **Nowack ECM, Grossman AR** (2012) Trafficking of protein into the recently established photosynthetic
43 organelles of *Paulinella chromatophora*. *Proc. Natl. Acad. Sci. USA* **109**: 5340-5345

44 **Nowack ECM, Price DC, Bhattacharya D, Singer A, Melkonian M, Grossman AR** (2016) Gene transfers
45 from diverse bacteria compensate for reductive genome evolution in the chromatophore of
46 *Paulinella chromatophora*. *Proc. Natl. Acad. Sci. USA* **113**: 12214-12219

47

1 **Oakley AJ, Coggan M, Board PG** (2010) Identification and characterization of gamma-glutamylamine
 2 cyclotransferase, an enzyme responsible for gamma-glutamyl-epsilon-lysine catabolism. *Journal of Biological Chemistry* **285**: 9642-9648

3 **Oberleitner L, Perrar A, Macorano L, Huesgen PF, Nowack ECM** (2022) A bipartite chromatophore
 4 transit peptide and N-terminal protein processing in the *Paulinella* chromatophore. *Plant Physiology* **189**: 152-164

5 **Oberleitner L, Poschmann G, Macorano L, Schott-Verdugo S, Gohlke H, Stühler K, Nowack ECM** (2020)
 6 The puzzle of metabolite exchange and identification of putative octotrico peptide repeat
 7 expression regulators in the nascent photosynthetic organelles of *Paulinella chromatophora*.
 8 *Frontiers in Microbiology* **11**: 607182

9 **Pei JM, Kim BH, Grishin NV** (2008) PROMALS3D: a tool for multiple protein sequence and structure
 10 alignments. *Nucleic Acids Research* **36**: 2295-2300

11 **Petoukhov MV, Franke D, Shkumatov AV, Tria G, Kikhney AG, Gajda M, Gorba C, Mertens HDT, Konarev PV, Svergun DI** (2012) New developments in the ATSAS program package for small-angle scattering data analysis. *Journal of Applied Crystallography* **45**: 342-350

12 **Schägger H** (2006) Tricine-SDS-PAGE. *Nature Protocols* **1**: 16-22

13 **Singer A, Poschmann G, Mühlich C, Valadez-Cano C, Hänsch S, Rensing SA, Stühler K, Nowack ECM**
 14 (2017) Massive protein import into the early evolutionary stage photosynthetic organelle of the
 15 amoeba *Paulinella chromatophora*. *Current Biology* **27**: 2763-2773

16 **Sørensen MES, Stiller ML, Kröninger L, Nowack ECM** (2025) Protein import into bacterial
 17 endosymbionts and evolving organelles. *FEBS Journal* **292**: 2992-3013

18 **Steiner JM, Löffelhardt W** (2002) Protein import into cyanelles. *Trends in Plant Science* **7**: 72-77

19 **Svergun D, Barberato C, Koch MH** (1995) CRYSL - A program to evaluate X-ray solution scattering of
 20 biological macromolecules from atomic coordinates. *Journal of Applied Crystallography* **28**: 768-773

21 **Svergun DI** (1992) Determination of the regularization parameter in indirect-transform methods using
 22 perceptual criteria. *Journal of Applied Crystallography* **25**: 495-503

23 **Tria G, Mertens HDT, Kachala M, Svergun DI** (2015) Advanced ensemble modelling of flexible
 24 macromolecules using X-ray solution scattering. *Iucrj* **2**: 207-217

25 **Williamson MP** (1994) The structure and function of proline-rich regions in proteins. *Biochemical Journal* **297**: 249-260

26 **Wróblewski K, Zalewski M, Kuriata A, Kmiecik S** (2025) CABS-flex 3.0: an online tool for simulating
 27 protein structural flexibility and peptide modeling. *Nucleic Acids Research* **53**: W95-W101

28

29

30

31

32

33

34

35 Figure Legends

36 **Figure 1: CrTP_{part2} adopts a structured fold. (A)** Multiple sequence alignment of 9
 37 representative crTP sequences (ClustalX2, manually refined). Identifiers of proteins that were
 38 experimentally studied are highlighted in color. In crTP_{part1}, conserved hydrophobic helix and
 39 adapter protein complex 1 binding site (AP-1 BS) are indicated. In crTP_{part2}, secondary structure
 40 elements resolved by X-ray crystallography are provided underneath the alignment. Interacting
 41 Cys residues are indicated by asterisks. Conserved hydrophobic aa involved in the interaction
 42 between arm and core are marked by arrow heads. **(B-C)** Cartoon representation of crystal
 43 structure of crTP_{part2_RnAH} (B; pdb id 9l09) and crTP_{part2_ArgC} (C; pdb id 9l08). Flexible arm, blue;
 44 structured core, gold. **(D)** Superposition of the cores of crTP_{part2_RnAH} (blue; Leu114 to Gln220)
 45 and crTP_{part2_ArgC} (green; Pro93 to Gln181). **(E)** Disulfide bridge between Cys113 and Cys169

1 (red) stabilizes the β -barrel of crTP_{part2_RnaH}. In the “open conformation”, extension of the flexible
 2 arm results in exposure of hydrophobic aas (orange). **(F)** In the “closed conformation” of
 3 crTP_{part2_ArgC}, the flexible arm interacts with the core via hydrophobic interactions (aas marked in
 4 orange).

5

6 **Figure 2: SAXS refined models of the analyzed proteins.** **(A)** The crTP_{part2_RnaH} core from the
 7 crystal structure is shown as orange cartoon and the solved part of the N-terminal arm as blue
 8 sphere representation. The core remained rigid for the EOM analysis and only the N and C-
 9 terminal parts were completed and used as flexible tails for the modeling. For clarity, only the N-
 10 terminal part is shown in sphere representations (volume fractions in green 22%, yellow 56%,
 11 cyan 11%, and magenta 11%). **(B)** Volume fractions from the crTP_{part2_RnaH} EOM analysis in the
 12 corresponding color code shown as spheres in (A). **(C)** EOM models of crTP_{part2_RnaH}-RnaH. The
 13 RnaH core (orange) was used as rigid body. The solved crystal structure of crTP_{part2} was used
 14 as flexible template and the missing linker regions were remodeled with EOM. **(D)** Dimer model
 15 of crTP_{part2_ArgC}-ArgC. The ArgC protomer dimer interface (grey and orange) was used as rigid
 16 body and the solved crTP_{part2} as flexible template. The flexible linkers and crTP_{part2} are colored
 17 in green and cyan for each protomer. The corresponding volume fractions are indicated below
 18 of each model in (C) and (D).

19

20 **Figure 3: ML tree depicting the inferred phylogenetic relationship between the structured core**
 21 **of crTP_{part2} and members of the GGCT-like superfamily.** Ultrafast bootstrap values ≥ 95 are
 22 shown at branches. Eukaryotic sequences are in black, bacterial in orange, archaeal in blue.
 23 Protein structures available are represented as cartoon models in which the part that is
 24 structurally similar to the crTP_{part2} structured core is highlighted in colors. Note that the *B. subtilis*
 25 homolog of BtrG (named YkqA, of unknown function; pdb id 2qik) contains two cyclotransferase
 26 domains within one polypeptide chain. Only the second is shown here and in Fig. S13. Species
 27 abbreviations: At, *A. thaliana*; Bs, *B. subtilis*; Ce, *C. elegans*; Dm, *Drosophila melanogaster*; Dr,
 28 *Danio rerio*; Ec, *E. coli*; Gg, *Gallus gallus*; Hs, *H. sapiens*; Mj, *Methanocaldococcus jannaschii*
 29 DSM; Mm, *Mus musculus*; Nc, *Niella circulans*; Os, *Oryza sativa*; Pf, *Pyrococcus furiosus*; Ph,
 30 *Pyrococcus horikoshii*; Sc, *S. cerevisiae*; Vc, *Vibrio cholerae*; Xl, *Xenopus laevis*; Yp, *Yersinia*
 31 *pestis*. **(B-D)** Superposition of the substrate-binding pocket of the human GGACT (pdb id: 3juc,
 32 violet with single residues highlighted in magenta) in complex with the product 5-oxoproline
 33 (shown in blue) and the one of crTP_{part2_ArgC} (green with single residues highlighted in light
 34 green). **(C)** Detail showing the conserved Tyr and Gly of the YGSL motif highlighted as well as
 35 other conserved or conservatively replaced hydrophobic side chains facing the substrate-
 36 binding pocket. **(D)** Detail showing the replacement of the catalytic Glu82 typical for GGCT-like
 37 proteins by a Tyr in crTP_{part2_ArgC}.

38

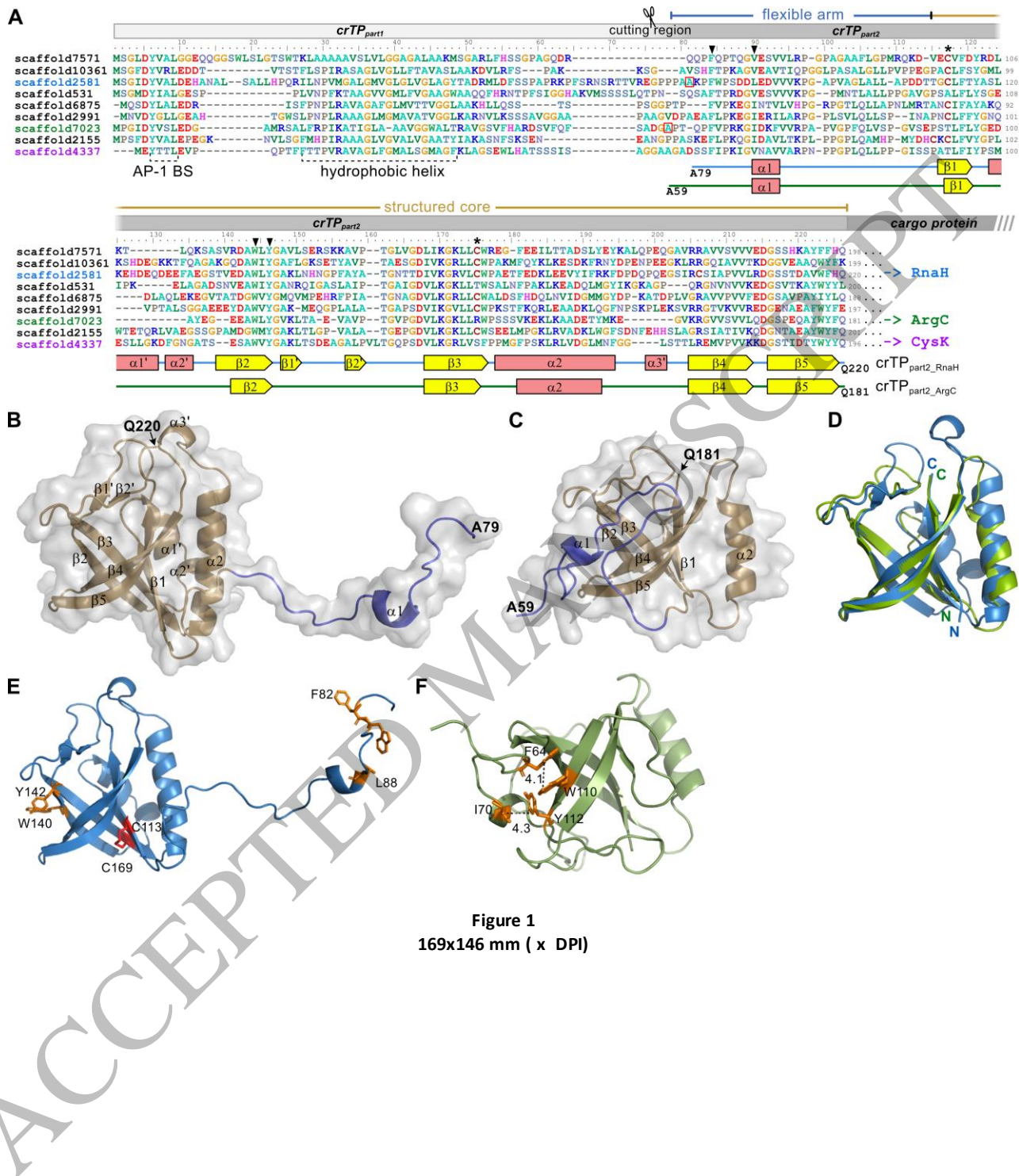
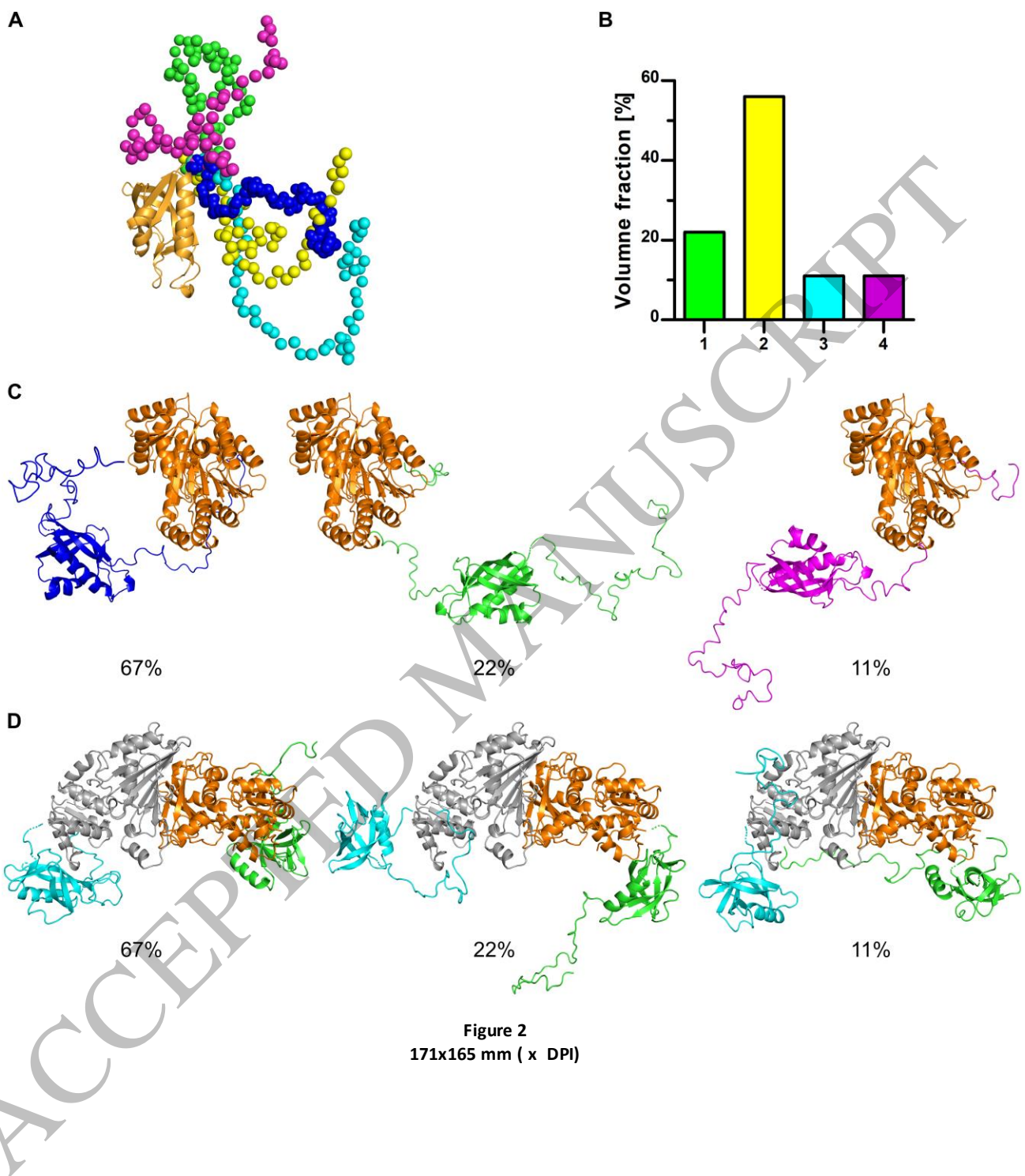


Figure 1
169x146 mm (x DPI)



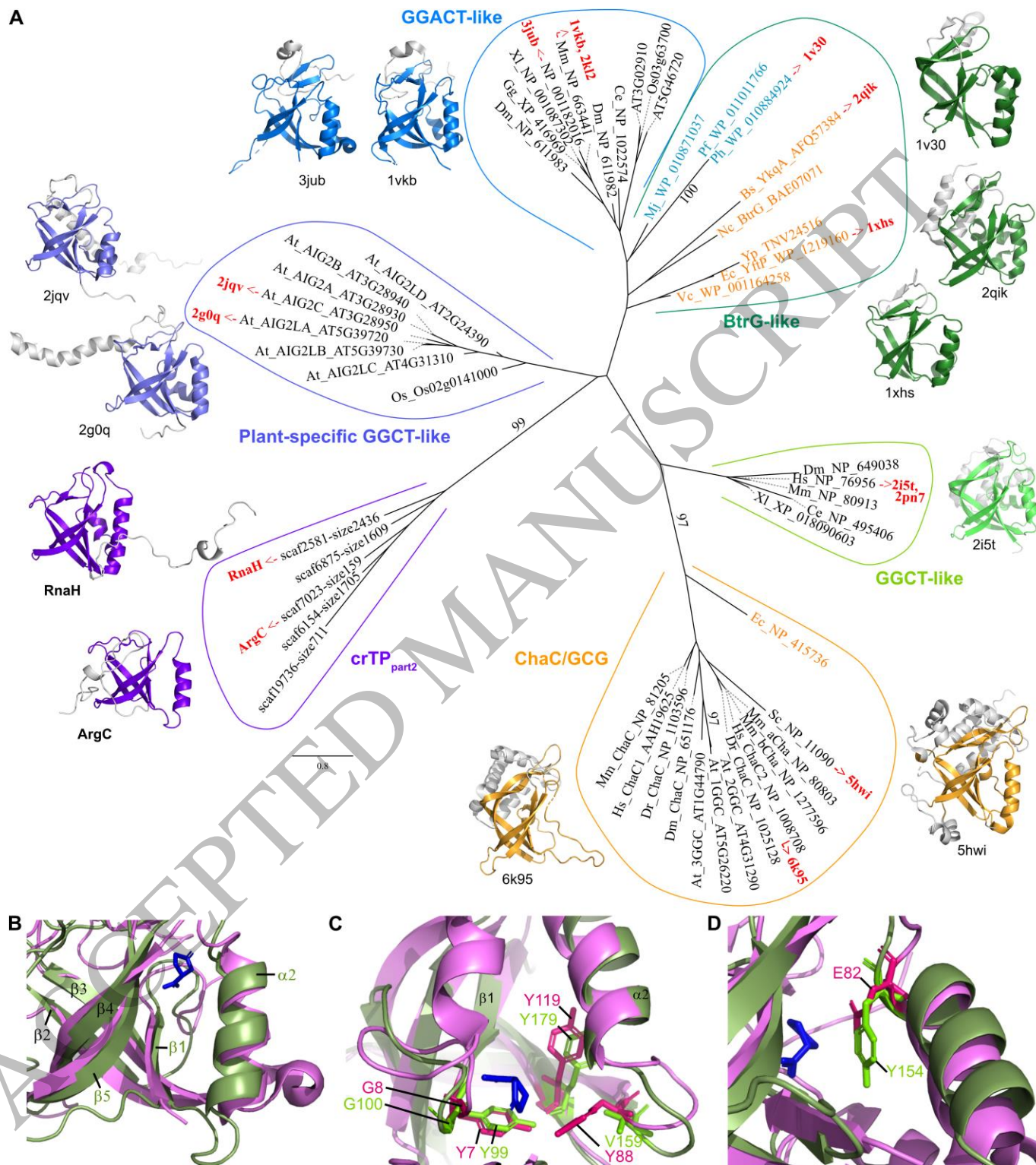


Figure 3
181x205 mm (x DPI)